The Frequency Response Analysis of a Wetted Wall Adiabatic Humidifier

DUANE F. BRULEY and JOHN W. PRADOS

The University of Tennessee, Knoxville, Tennessee

This paper describes a theoretical and experimental analysis of dynamic adiabatic humidification in a wetted wall column.

The adiabatic humidification conditions, together with the large heat capacity and transfer rates in the liquid phase, relative to those in the gas phase, insured a constant liquid and interfacial temperature in the column. Hence the mathematical model could be simplified to consideration of the air phase alone. Partial differential equations describing temperature-time-distance relations were derived for the system under laminar and turbulent air flow conditions. The desired solution of these equations was an analytical expression for the open loop air-temperature transfer function of the system. In this investigation an analytical expression for the turbulent flow model was obtained; however in the laminar flow case it was found advisable to solve the defining equations numerically on the digital computer.

The mathematical process models were tested experimentally by the frequency response technique (*1*). In frequency response studies of humidifier dynamics the input gas-phase temperature was forced to vary in sinusoidal manner with frequency ω. If the incoming water temperature is held constant, the output air temperature will, after an initial transient, also vary sinusoidally with the same frequency ω but with different amplitude and phase than the input sine wave if the system under consideration is a linear system. The ratio of output to input amplitudes M and the phase shift of output sine wave relative to input wave ϕ are functions of frequency alone for a given stable, linear system. The curves of M and ϕ as functions of the forcing frequency ω, known as Bode plots (*1*), can be used to characterize linear system dynamics completely, since an input wave of arbitrary shape can be represented as a Fourier sine series and the corresponding Fourier series for the output developed from the frequency response functions $M(\omega)$ and $\phi(\omega)$ (*5*).

Direct sinusoidal forcing of the inlet gas temperature was employed in the present study, and inlet and outlet air temperature sinusoids were recorded as functions of time.

EXPERIMENTAL INVESTIGATION

Equipment

A flow diagram illustrating the air and water flow systems for the wetted wall column and auxiliary equipment is shown in Figure 1.

Compressed air flowed into a standard metal oxygen cylinder, used as a stabilizing tank, thence through a two-stage pressure regulator and two calcium chloride desiccant beds, constructed from 13-in. lengths of 2-in. schedule 40 pipe in series.

The air then passed through a wet-and-dry-bulb humidity indicator and into the heating section which consisted of a 12-in.-long, 1-in. diameter Pyrex glass pipe flanged to a Pyrex glass cross. At this point a harmonic temperature variation was generated by the motion of a brass cartridge heater ½ in. in diameter and 10 in. long, connected to a scotch yoke (*4, 6*) drive.

The air then flowed through a 1-in. diameter, 4-ft.-long Plexiglas inlet section to ensure a developed velocity profile at the inlet to the column. A scale drawing of the 1-in. diameter, 1.5-ft.-long Plexiglas wetted wall column is shown in Figure 2. At the outlet of the column the air flowed through another wet-and-dry-bulb temperature indicator and finally to an air flow rotameter.

Water was supplied to the column from a constant head tank through a rotameter, into the water jacket, and over a weir wetting the wall of the column inner tube and contacting the air flowing countercurrent up the center of the tube. Some of the water was trapped in a basin at the bottom of the column to eliminate air leakage from the water outlet.

Copper-constantan thermocouples were located at the water and air inlets and outlets. The air temperature couples were connected through a cold junction bottle and selector switch to a low level preamplifier with zero suppression. Temperature-time charts were recorded on a single-channel recorder. Water temperature thermocouples were connected through the cold junction bottle directly to a potentiometer.

Procedure

The column was aligned vertically by the use of a steel hoop with set screws and a plumb bob. After the constant

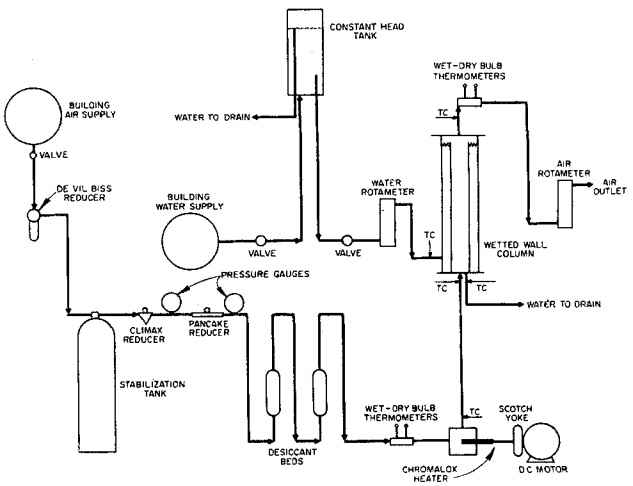

Fig. 1. Schematic diagram of air-water flow systems.

* Duane F. Bruley is now at Clemson College, Clemson, South Carolina.

head tank was filled the drain valve at the bottom of the heating section was opened, the water valve at the inlet to the column was opened until complete wetting of the wall was attained. The water flow rate was then adjusted to minimize the effect of rippling on surface area and still maintain complete wetting of the column. Rippling begins at a Reynolds number of about 25 for falling liquid films (9); however for water the increase in surface area is only a few per cent up to a Reynolds number of about 600. The maximum liquid Reynolds number used in this investigation was 566 for the turbulent air flow runs. For the laminar flow runs the liquid Reynolds number was about 400.

For the laminar flow runs the air Reynolds number was adjusted to 778 based on an average air flow velocity relative to the wall. In turbulent flow the Reynolds number was about 2,500 based on the average air flow velocity relative to the wall. To ensure that standard velocity profiles for laminar and turbulent flow actually existed tests were conducted by introducing cigarette smoke at the base of the calming section and visually observing the flow conditions in the column. For laminar flow the smoke appeared first at the center line of the column, then filled the entire wetted wall tube smoothly, and finally cleared from the center line to the wall. For the turbulent case the smoke entered and left the column as a well-mixed slug. Radial temperature profiles also supported the existence of the standard velocity profiles.

A powerstat controlling the cartridge heater was then set and the heater inserted all of the way into the heating section. After the inlet section was completely dried a variable speed d.c. motor controller was set at the desired frequency and allowed to operate under these conditions until steady state was established.

Column inlet and outlet temperature-time (see Figure 3) plots were made over a frequency range from 18 to 1,380 cycles/hr. Bode plots were developed by plotting the ratio of outlet to inlet sine wave amplitudes M vs. frequency and the angular shift between output and input sine waves ϕ vs. frequency.

Recordings were made at the column center line and at the midpoint, half way between the center line and the column wall.

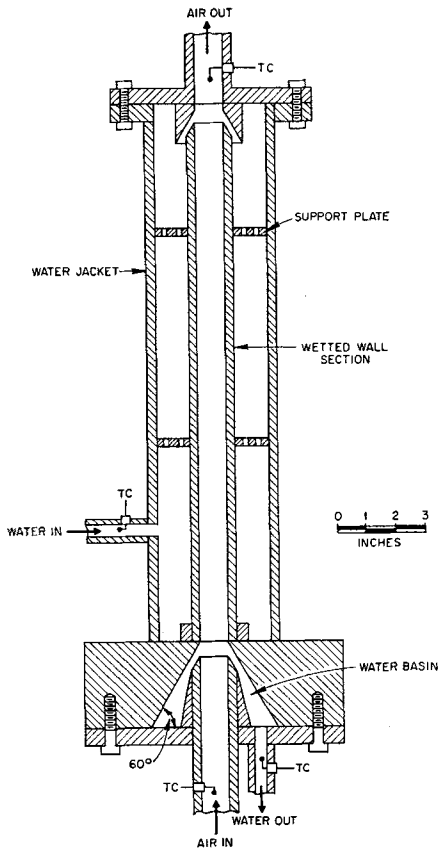

Fig. 2. Cross-sectional view of column.

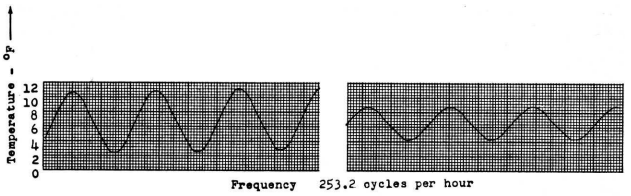

Fig. 3. Center-line recorder temperature traces, turbulent flow.

THEORETICAL INVESTIGATION

As previously noted, the conditions of adiabatic humidification lead to a uniform water temperature during steady state operation. In addition the high heat capacity and rate of heat transfer in the water phase, relative to those in the gas phase, prevent the interface and bulk water temperatures from fluctuating more than a fraction of a degree during the sinusoidal dynamic operation in this investigation. Hence the mathematical models can be restricted to the air phase alone, with a boundary condition of constant temperature at the air-water interface.

Laminar Air Flow Model

The differential equation describing the unsteady state thermal behavior of the air phase are based on the following assumptions:

1. Velocity gradients are small enough so that the terms related to viscous dissipation can be neglected.
2. Velocity components are in the x direction only.
3. The use of average values for density, viscosity, and thermal conductivity is valid.
4. Temperature is a function of r, x, and time only (axial symmetric system).
5. No axial conduction occurs.

The equation can be written as

$$\frac{\partial t}{\partial \theta} = \frac{\alpha}{r}\frac{\partial}{\partial r}\left(r\frac{\partial t}{\partial r}\right) - v\frac{\partial t}{\partial x} \tag{1}$$

for

$$x > 0 \qquad R > r \geq 0$$

where the limiting conditions can be written as

$$\frac{\partial t}{\partial r}(0, x, \theta) = 0 \quad t(R,x,\theta) = 0$$
$$t(r, 0, \theta) = t_o \qquad t(r,x,0) = 0 \tag{2}$$

The standard parabolic velocity was assumed to describe the local velocity as observed earlier by Gilliland and Sherwood (3) and supported by smoke tests in the present investigation:

$$v = V_o\left[1 - \left(\frac{r}{R}\right)^2\right] \tag{3}$$

The dependent variable t is the deviation from the steady state temperature with a value of zero at $\theta = 0$ so that the resulting Laplace-transformed dynamic equation is

$$S\bar{t} = \alpha\left[\frac{\partial^2 \bar{t}}{\partial r^2} + \frac{1}{r}\frac{\partial \bar{t}}{\partial r}\right] - v\frac{\partial \bar{t}}{\partial x} \tag{4}$$

This problem has been treated by Farrell and Leonard (2) in terms of residence time distributions. However for comparison with results from the present experiments it was more convenient to solve the problem in the frequency domain.

This required the simultaneous solution of two partial differential equations; however each equation contained only two independent variables at a given frequency. The following analysis shows the development of the fre-

quency-domain equations from the original partial differential equation.

Now denote the transfer function for the wetted wall column by the complex number $G'(r, x, S)$, so that

$$\bar{t} = \bar{t}_o\, G'(r, x, S) \tag{5}$$

It has been established (*1*) that the harmonic response function of a given system can be obtained from the system transfer function by replacing the Laplace transform variable S by the pure complex number $i\omega$, where ω is frequency. Therefore substitution of $i\omega$ for S yields

$$\bar{t} = \bar{t}_o\, G'\,(r,x,i\omega) = \bar{t}_o\,[P(r,x,\omega) + iQ(r,x,\omega)] \tag{6}$$

Substitution into the differential equation and separation of the result into real and imaginary components gives

$$\left\{ \omega Q + \alpha \left[\frac{\partial^2 P}{\partial r^2} + \frac{1}{r}\frac{\partial P}{\partial r} \right] - v\frac{\partial P}{\partial x} \right\} +$$

$$i\left\{ -\omega P + \alpha \left[\frac{\partial^2 Q}{\partial r^2} + \frac{1}{r}\frac{\partial Q}{\partial r} \right] - v\frac{\partial Q}{\partial x} \right\} = 0 \tag{7}$$

Since a complex number is zero if and only if its real and imaginary components both vanish, the terms in braces in the above equation may each be set equal to zero, thence forming two partial differential equations with dependent variables P and Q.

The boundary conditions for the case of uniform input can be written as

$$\frac{\partial P}{\partial r} = \frac{\partial Q}{\partial r} = 0 \text{ at } r = 0 \tag{8}$$

$$\begin{aligned} P(R,x,\omega) &= Q(R,x,\omega) = 0 \quad \text{at} \quad r = R \\ P(r,0,\omega) &= 1 \text{ at } x = 0 \\ Q(r,0,\omega) &= 0 \text{ at } x = 0 \end{aligned}$$

Boundary conditions for the case of radially dependent input are as above, except that the inlet phase shifts and amplitude ratios, with respect to the center line, were experimentally determined functions of radius.

The two simultaneous partial differential equations were solved with the Crank-Nicholson six point implicit differencing technique (*8*). The mesh model used for the numerical calculations is the same as that presented by Von Rosenberg, Durrell, and Spencer (*10*). This model eliminates the need for a special center-line equation since the mesh points are displaced ½ increment from the boundaries in the r direction so that the following quantities define the r and x positions:

$$v_j = (j - \tfrac{1}{2})\,\Delta r \quad 1 \leq j \leq J \quad \Delta r = \frac{R}{J} = h \tag{9}$$

$$x_i = i\Delta x \qquad 1 \leq i \leq I \quad \Delta x = \frac{X}{I} = k \tag{10}$$

Theoretical amplitude ratios and phase shifts can be obtained from P and Q at the column outlet through the relations

$$M(\omega) = \sqrt{P^2 + Q^2} \tag{11}$$

$$\phi(\omega) = \tan^{-1}\left(\frac{Q}{P}\right) \tag{12}$$

Letting P and Q at the fictitious point $j = 0$ be the same as at $j = 1$ satisfies the boundary conditions at the center line $j = \tfrac{1}{2}$, since it forces the derivatives of P and Q, with respect to r, to be zero. The boundary conditions at the wall were satisfied by making $P = Q = 0$ in the $J + 1$ position.

The two differenced equations can be described by a system of linear algebraic equations represented in matrix notation by tridiagonal coefficient matrices. The matrix equations were solved on an IBM-1620 digital computer with a method outlined by Bruce et al. (*8*) as due to Thomas. Solutions were obtained both for uniform and for radially varying temperatures at the column inlet.

Turbulent Air Flow Model

The differential equation describing the unsteady state thermal behavior of the air phase is based on the following assumptions:

1. Velocity and temperature profiles are uniform (complete mixing).
2. Mass velocity is constant.
3. Film theory applies.
4. All resistance to heat and mass transfer is in the gas film.

The equation can be written as

$$\frac{\partial t}{\partial \theta} = -\frac{G}{\rho}\frac{\partial t}{\partial x} - \frac{2h}{\rho s R}\,t \tag{13}$$

Laplace transformation, integration, and substitution of the inlet and outlet boundary conditions

$$\begin{aligned} \bar{t}\,(x = 0) &= \bar{t}_1 \\ \bar{t}\,(x = X) &= \bar{t}_o \end{aligned} \tag{14}$$

results in

$$\frac{\bar{t}_o}{\bar{t}_1} = e^{-\frac{2hX}{sRG}}\, e^{-\rho\frac{SX}{G}} \tag{15}$$

Substitution of the pure imaginary number $i\omega$ for S yields the desired amplitude ratio and phase shift directly. For this case the amplitude ratio was found to be independent of the frequency and can be written as

$$M = e^{-\frac{2hX}{sRG}} \tag{16}$$

The phase shift is equivalent to that for pure transport delay and can be represented by

$$\phi = \frac{\rho\omega X}{G} \tag{17}$$

These results have been obtained by other investigators (*4, 6*) for single-phase, slug flow systems.

PRESENTATION OF RESULTS

The mechanical harmonic temperature generator, designed for this investigation, limited the frequency range that could be analyzed. It produced reasonable temperature sinusoids over the frequency range of 18 to 1,380 cycles/hr.

Theoretical calculations were made for the 1.5 ft. wetted wall section. For valid comparison of the experimental and theoretical results it was necessary to correct the original experimental data by determining the amplitude ratio and phase shift for the combined inlet-outlet section.

For linear systems the total amplitude ratio represents the product of the individual component amplitude ratios, and the total phase shift represents the sum of the individual phase shifts. Therefore the wetted wall section amplitude ratios were calculated with the following equation:

$$\text{Wetted wall section amplitude ratio} = \frac{\text{Total column amplitude ratio}}{\text{Inlet-outlet section amplitude ratio}} \tag{18}$$

Phase shift corrections for excess length (about 6 in.) were approximated by pure transport delay.

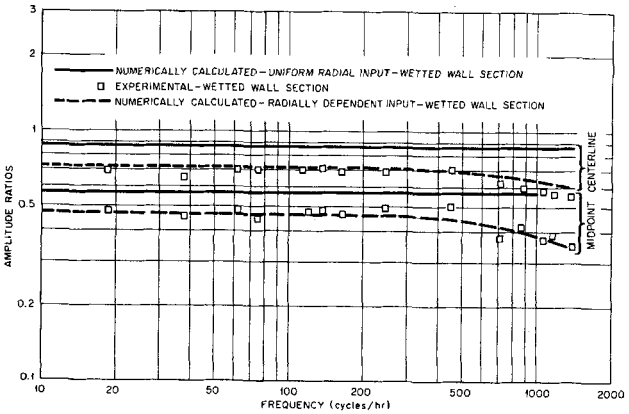

Fig. 4. Amplitude ratios vs. frequency, laminar flow.

In the laminar flow region it was necessary to consider an entrance length correction for the original experimental phase shift at the midpoint, since the data were taken by positioning both the inlet and outlet thermocouples at the midpoints. For comparison with the calculated results the inlet thermocouple should have been placed at the center line, since the theoretical models were evaluated with reference to the center line. To correct for this the relative phase shift between the midpoint and center line at the column inlet was calculated for pure transport delay in the inlet section with the following equation:

$$\phi_c = \omega l' \ 360 \left[\frac{1}{V_o} - \frac{1}{v_m} \right] \qquad (19)$$

Physical properties were evaluated at the mean temperature of the fluid under consideration. The air mean temperature was 113°F. for the laminar flow case and 100°F. for the turbulent flow case. The water temperature was constant over the column length at 66°F. for both cases.

The water flow rate for the laminar case was 1.19 lb./min. The volumetric air flow at 113°F. and atmospheric pressure for the laminar case was 33 cu.ft./hr., while for the turbulent case at 100°F. and atmospheric pressure the flow rate was 104 cu.ft./hr.

For the case of uniform temperature and zero phase shift at the inlet to the wetted wall section the numerical model was solved at zero frequency and compared with the first three terms of the steady state theoretical solution developed by Graetz (7). At the center line there was 0.83% difference and at the midpoint 2.92% difference in the calculated values of temperature ratio based on the

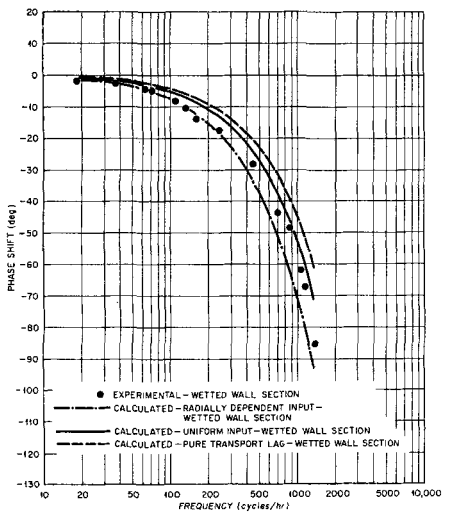

Fig. 5. Center-line phase shift vs. frequency, laminar flow.

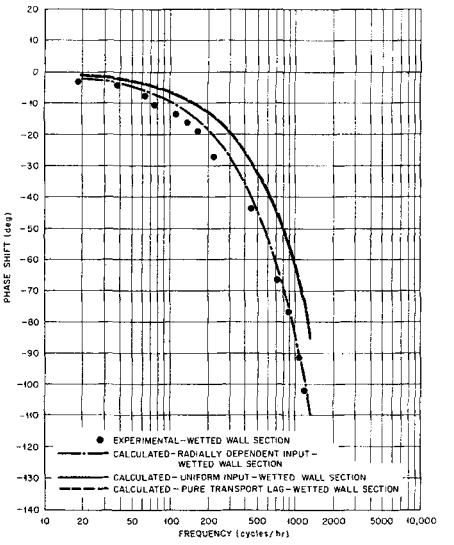

Fig. 6. Midpoint phase shift vs. frequency, laminar flow.

numerical solution. Of course for both cases the phase shift was found to be zero. This provides an analytical check on the numerical calculations.

Laminar Air Flow

In Figure 4 the center line and midpoint experimental wetted wall section amplitude ratios are compared with those obtained from the numerical solution of the laminar flow theoretical model. The numerical solution was obtained for two sets of input conditions, the case of uniform radial temperature input data and the case of radially dependent temperature input data. As shown the uniform input case amplitude ratio is nearly constant over the frequencies investigated, and the amplitude ratios are from 20 to 60% greater than those from the experimental investigation or from the case of radially dependent input.

In Figures 5 and 6 for the center line and midpoint, respectively, the experimental wetted wall section phase shifts are compared with those determined numerically with the laminar flow theoretical model and with the phase shift due to pure transport delay. These plots show that the experimental phase shift agrees well with the calculated results based on the radially dependent input data.

Turbulent Air Flow

Figure 7 compares the center line and midpoint experimental amplitude ratios for the wetted wall section with the calculated analytical results. In accordance with the assumption of plug flow all of the experimental points should be on the same straight line, $M = 0.62$. This value was obtained from Equation (17) based on the heat trans-

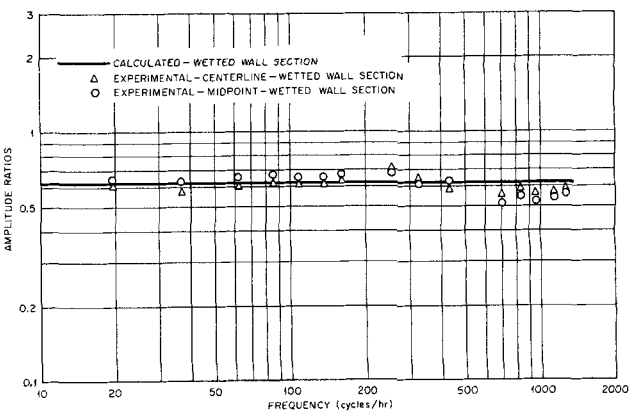

Fig. 7. Turbulent amplitude ratios vs. frequency.

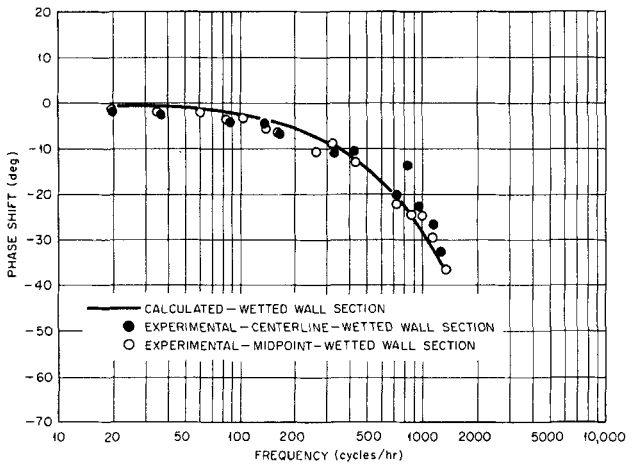

Fig. 8. Turbulent phase shift vs. frequency.

fer coefficient determined from an equation developed by Gilliland and Sherwood (3) for general applicability under conditions of turbulent gas flow in wetted wall towers.

It is apparent that the experimental deviation from the analytical solution is greater at the higher frequencies. This might be due to the difficulty in measuring accurately the smaller amplitudes generated at the higher frequencies.

In Figure 8 the experimental center line and midpoint phase shifts are compared with the theoretical phase shift based on the turbulent model. The theoretical phase shift was that of pure transport delay.

CONCLUSIONS

The following conclusions may be drawn from a wetted wall adiabatic humidifier under the conditions of the present experiments:

1. The plug flow mathematical model describes well the turbulent flow frequency response characteristics of the column.
2. Turbulent flow magnitude ratios are essentially constant over the range of frequencies investigated.
3. Turbulent flow phase shift is that of pure transport delay in the frequency range investigated.
4. The viscous flow, parabolic velocity profile mathematical model, with radially dependent temperature input, describes well the laminar flow frequency response characteristics of the column.
5. The viscous flow, parabolic velocity profile mathematical model, with uniform radial temperature input, does not accurately describe the laminar flow frequency response characteristics of the column.
6. Laminar flow phase shift is influenced by heat transfer effects as well as transport delay.
7. Liquid velocity has little effect on the laminar or turbulent flow characteristics for a column with a small length to diameter ratio such as the one used in this investigation.
8. The inlet and outlet sections of operational equipment can have a significant influence on the overall equipment dynamic behavior.
9. Mass transfer has very little effect on the theoretical prediction of the dynamic heat transfer behavior under conditions of adiabatic humidification.
10. The numerical solution of a partial differential equation involving three independent variables in the time domain can be simplified by reducing the equation to a pair of simultaneous partial differential equations involving only two independent variables in the frequency domain.

ACKNOWLEDGMENT

The authors are very grateful to the Texaco Foundation and the Shell Foundation for the support of this work.

NOTATION

G = mass velocity of air, lb./(hr.)(sq.ft.)
G' = open loop transfer function
h = convective conductance, B.t.u./(hr.)(sq.ft./°F.) or radial increment size, ft.
I = total number of axial increments
i = $\sqrt{-1}$ or axial increment subscript
J = radial increment subscript
j = total number of radial increments
k = axial increment size, ft.
l' = entrance length, ft.
M = amplitude ratio
P = real part of complex transfer function
Q = imaginary part of complex transfer function
R = pipe radius, ft.
r = variable radius, ft.
S = Laplace transform complex variable
s = humid heat capacity, B.t.u./(lb. dry air)(°F.)
t = dynamic temperature (deviation from steady state value), °F.
$\bar{t}$ = Laplace transformed temperature
$\bar{t}_1$ = Laplace transformed temperature, in.
$\bar{t}_0$ = Laplace transformed temperature, out (turbulent case) or center-line temperature at, $x = 0$ (laminar case)
V_0 = center-line velocity, ft./hr.
v_m = midpoint velocity, ft./hr.
v = local velocity, ft./hr.
X = column height, ft.
x = variable axial distance, ft.

Greek Letters

α = thermal diffusivity, sq.ft./hr.
Δr = radial increment size, ft.
Δx = axial increment size, ft.
θ = time, hr.
ρ = density, lb./cu.ft.
ϕ = phase shift, deg.
ϕ_c = midpoint phase shift relative to the center line at the column inlet, deg.
ω = frequency, rad./hr. or cycles/hr.

LITERATURE CITED

1. D'Azzo, J. J., and C. H. Houpis, "Feedback Control System Analysis and Synthesis," McGraw-Hill, New York, (1960).
2. Farrell, M. A., and E. F. Leonard, *A.I.Ch.E. Journal*, **9**, 190 (1963).
3. Gilliland, E R., and T. K. Sherwood, *Ind. Eng. Chem.*, **26**, 516-23 (1934).
4. Gray, R. I., and J. W. Prados, *A.I.Ch.E. Journal*, **9**, 211 (1963).
5. Hougan, J. O., and R. A. Walsh, *Chem. Eng. Progr.*, **57**, No. 69 (1961).
6. Keyes, J J., *A.I.Ch.E. Journal* **1**, 305 (1955).
7. Knudsen, J. G., and D. L. Katz, "Fluid Dynamics and Heat Transfer," McGraw-Hill, New York (1958).
8. Lapidus, L., "Digital Computation for Chemical Engineers," McGraw-Hill, New York (1961).
9. Tailley, S. R., and S. Partalski, *Trans. Inst. Chem. Eng. 16*, 38, 324 (1960).
10. von Rosenberg, D. V., P. L. Durrill, and E. H. Spencer, "Numerical Solution of Partial Differential Equations Representing Fixed Bed Reactions," Esso Research Laboratories, Baton Rouge, La., unpublished.

Manuscript received July 10, 1963; revision received February 28, 1964; paper accepted March 2, 1964; paper presented at A.I.Ch.E. Houston meeting.